Pixel-RRT*: A Novel Skeleton Trajectory Search Algorithm for Hepatic Vessels

Jianfeng Zhang[1,2], Wanru Chang[1,2], Fa Wu[3], Dexing Kong[1,2,†]
[1]School of Mathematical Sciences, Zhejiang University, Hangzhou, China
[2]Institute of Applied Mathematics and Image Processing, Zhejiang University, Hangzhou, China
[3]Demetics Medical Technology Co., Ltd, Hangzhou, China
{jfzhang2018, 11935029}@zju.edu.cn 66751168@qq.com dxkong@zju.edu.cn

***Abstract*—In the clinical treatment of liver disease such as tumor, the acquisition of vascular skeleton trajectory is of great worth to untangle the basin and venation of hepatic vessels, because tumor and vessels are closely intertwined. In most cases, skeletonization based on the results of vascular segmentation will be prone to fracture due to the discontinuous segmenting results of vessels. As the overall tree-like system of hepatic vessels is a thin tubular tissue, we expect to start the analysis of vessels from vascular skeleton to vascular boundary, not the contrary, which can more effectively implement the image computing of hepatic vessels and interpret the tree-like expansion. To this issue, in this paper, we propose an innovative approach Pixel-RRT* inspired by Marray's Law and the growing rule of biological vasculature. It can be applied to the skeleton trajectory search for the intricate hepatic vessels. In Pixel-RRT*, we introduce the novel pixel-based cost function, the design of pixel-distributed random sampling, and a multi-goal strategy in the shared graph of random tree based on the general algorithmic framework of RRT* and RRT. Without any prior segmentation of the vessels, the proposed Pixel-RRT* can rapidly return the rationally bifurcated vascular trajectories satisfying the principle of minimal energy and topological continuity. In addition, we put forward an adaptively interpolated variational method as the postprocessing technique to make the vascular trajectory smoother by the means of energy minimization. The simulation experiments and examples of hepatic vessels demonstrate our method is efficient and utilisable. The codes will be made available at https://github.com/JeffJFZ/Pixel-RRTStar.**

***Index Terms*—Pixel-RRT*, Skeleton Trajectory, Minimal Energy, Topological Continuity**

I. Introduction

The analysis of the vascular system in biomedical images is still a tough task, due to the high complexity of topological structure [1]–[3]. Concretely, we choose hepatic vessels as the typical case. In the process of clinical diagnosis, the accurate segmentation of hepatic vessels, and the precise definition of the corresponding topology are of great significance for the implementation of liver disease diagnosis and treatment plan. According to the obtained information of vessels, doctors can more accurately perform preoperative planning, intraoperative navigation, and postoperative evaluation. However, the tree-like structure of the hepatic vessel system is excessively intricate, and the noise of the image data has a noticeable impact on the imaging quality of small blood vessels. Local variability of vessels, poor visibility of the vascular endings, and prone to fracture of the segmentation results, etc., making the extraction and trajectory analysis of the vascular skeleton has always been a valuable but challenging job.

Skeleton is devoted to describe the geometric characteristics of objects, and has the same topological information and shape features as the original target objects [4], hence it plays an important role in digital image analysis. It is widely used in computer vision [5], medical image visualization [6], feature extraction and representation [7], model matching and tracking [8], etc. Over the years, varieties of skeleton extraction algorithms have been proposed in the literature. Typically, most of them are based on minimal path approach [9]. Wink et al. [10] developed a multiscale vessel tracking to determine the skeleton on the basis of the minimum cost path program. In [11], Deschamps and Cohen extracted minimal paths in 3D images by fast marching methods. There are other methods of skeleton extraction have also been proposed, such as the parallel thinning algorithms [12], methods based on distance transform (Euclidean metric [13], Manhattan metric [14]), ridge computation method [15] and curve tracing algorithm [16]. Whereas these methods are sensitive to boundary noise or time-consuming, and they generally rely on the prior segmentation result of tubular objects to acquire the final centerline, which means that the quality of the segmentation directly influences the result of skeletonization, such as the discontinuous or ambiguous results.

Growth and bifurcation of vessels inside human organs look like the growing tree or the expanding river basins when we are not strictly talking about dimensions. In the process of their growth, the cost for transport and maintenance is minimized. This feature is also suitable for plants and even microorganisms, which is the origin of Murray's law [17]. The vasculature is indicated to be an optimal system for researchers' conducting quantitative analysis via mathematical topology [18]. Bruyninckx et al. [19], [20] presented some research cases on vessel segmentation by global optimization. The work of Ronellenfitsch et al. [21] further gave evidence of the global optimum and minimum energy principle of vasculature in biological systems, whose theory and experiments prove that the analysis of vessels combined with the homologous growth law and energy principle is a far-reaching research problem.

Rapidly-exploring Random Trees algorithm (RRT) [22],

[23] is a classical graph-related algorithm based on stochastic incremental sampling, which is widely applied to the motion planning of self-driving, kinematics, robots, games and hybrid systems [24]–[27]. Although the RRT algorithm yields an initial feasible solution, it is not an optimal solution. Karaman et al. [28] proposed a variant of RRT called the Rapidly-exploring Random Tree star (RRT*), which asymptotically finds the optimal path from starting point to ending point. Gammell et al. [29] proposed the Informed RRT*, which made a simple modification of RRT* by sampling nodes inside an ellipsoid. This method can find an optimum solution within tighter tolerances than RRT*, and improve the convergence rate and the quality of the final solution. Various variants of RRT* have been proposed to improve the computing efficiency and algorithm performance, such as IB-RRT* algorithm [30], potential guided directional-RRT* [31], adaptive potential guided directional-RRT* [32], RT-RRT* [33] and so on. Note that some classical methods similar with RRT*s for incremental search, such as A* [34] and Probabilistic Roadmaps (PRMs) [35], have a higher computational complexity than RRT*s. That is why researchers select RRT*-based methods to ensure real-time performance of the online informative path planning [36]. RRT*-based search algorithms satisfy the principle of energy minimum and global optimization, which will also be used for the vascular image analysis through our work.

In recent years, we have been exposed to a wealth of vascular problems and image data in our medical image computing projects, and gain a certain understanding of the vascular topology and growth model. Finally, inspired by Murray's law that the vascular system satisfies the principle of minimum energy, and thoughts of [21], we put forward a trajectory analysis and skeleton extraction algorithm Pixel-RRT* for the vascular images with a novel design of the pixel-based cost function. The classical RRT* family is usually used for real-time path planning, not image analysis, because the distance-based cost function of them is not able to represent the distribution and difference of image pixels. Compared with those classical RRT*-based methods, Pixel-RRT* can compute the cost distribution of a vascular image by redesigning the cost function combined with the varying image pixels. Our proposed method is based on the basic framework of RRT*, and then we design some specialized methods aimed at vascular images to optimize Pixel-RRT*. The algorithm does not require any image segmentation of the hepatic vessels in advance, only need to calibrate the starting point and ending point, so as to accurately find the whole or partial vascular skeleton trajectory. Meanwhile, it can avoid the problems caused by discontinuity, over-segmentation or under-segmentation of the results of vascular segmentation. Furthermore, the presented Pixel-RRT* supports the skeleton trajectory search aimed at multi-goals and can fast obtain all the trajectories with rational bifurcation nodes.

The paper is organized as follows. In Section II-A, we give a detailed description of Pixel-RRT*. The postprocessing technique is discussed in further depth in Section II-B. In Section III, we provide the effectiveness of the theoretical algorithms through practical experiments. In section IV, we draw some conclusions and put forward some future work in this research domain.

II. Methods

A. Pixel-RRT*

In this section, we describe our Pixel-RRT* in detail, which is demonstrated in Algorithm 1. In order to transfer the traditional RRT-based methods for motion planning over distance to our Pixel-RRT* for image-based trajectory analysis, we make reasonable redesign in three modules: pixel-distributed random sampling, pixel-based cost function (`PixelCost`) and multi-goal strategy based on the basic architecture of RRT* [23], [28].

In Algorithm 1, Pixel-RRT* can cope with the problem of multiple goals besides that of a single endpoint (Details in II-A3). Thus the input covers the image $\mathcal{M}$, the starting point x_{init}, and the single goal or multiple goals $x_{goal(s)}$. The other designs differing from RRT*, include `Pixel-distributedRandomSample` in Line 3 (What happened can be seen in II-A1) and `PixelCost` of Line 10 to Line 22 (Detailed exploration in II-A2). `ReachedWithAuto-convergence` in Line 29 is a universal design about convergence rate in numerical computing methods for automatically evaluating the reached path(s). The computation of `Cost` of Algorithm 1 is still the same as RRT*, which is the sum of cost from the comparing node to x_{init}. In Pixel-RRT*, the cost function turns into pixel-based cost instead of distance-based cost. Therefore, it will be adapted to become the summation of the new cost.

In the process of tree expanding and rewiring, Pixel-RRT* is chasing the global minimization all along, and eventually it return the minimum-cost trajectory from the starting point to the ending point. Pixel-RRT* is applicable to the two-dimensional and three-dimensional tasks uniformly, as the algorithm needs to change nothing but the dimension.

1) Pixel-distributed Random Sampling: The `Pixel-distributedRandomSample` function in Line 3 of Algorithm 1 uses the Equation (1), which is appended a probabilistic operator $\mathbb{P}_p$ based on the adopted preliminary design of Random Sampling in RT-RRT*. The probabilistic operator $\mathbb{P}_p$ is defined in Equation (2), varying with the absolute value of pixel difference between x_{rand} and P_0 (Equation (3)).

$$x_{rand}=\begin{cases}\mathtt{L}(x_{goal(s)})\bullet\mathbb{P}_p & if\ \mathfrak{p}_r > 1-a \\ \mathtt{U}(\chi)\bullet\mathbb{P}_p & if\begin{cases}\mathfrak{p}_r\leq\frac{1-a}{b}\ \ or \\ \nexists path(x_{init}, x_{goal(s)})\end{cases} \\ \mathtt{E}(x_{init}, x_{goal(s)})\bullet\mathbb{P}_p & otherwise\end{cases} \tag{1}$$

In Equation (1), $\mathfrak{p}_r$ is a random number between [0, 1], a, b are user-given constant variables similar with RT-RRT*. $\mathtt{L}(x_{goal(s)})$ samples randomly in the line between $x_{goal(s)}$ and the node closest to $x_{goal(s)}$. $\mathtt{U}(\chi)$ samples the search environment uniformly. $\mathtt{E}(x_{init}, x_{goal(s)})$ samples inside an ellipsis such that the path from x_{init} to $x_{goal(s)}$ is inside it. We refer readers to References [29], [33] for further details on how to choose the parameters and sample in the ellipsis.

Algorithm 1: Pixel-RRT*

Input: $\mathcal{M}$, x_{init}, $x_{goal(s)}$
Output: The path(s) Γ from x_{init} to $x_{goal(s)}$

$\mathbf{G} = (\mathbf{V}, \mathbf{E})$.Initialize();
for $k = 1$ *to* n **do**
  $x_{rand} \leftarrow$ Pixel-distributedRandomSample($\mathcal{M}$);
  $x_{closest} \leftarrow$ ClosestNeighbor(x_{rand}, $\mathbf{G}$);
  $x_{new} \leftarrow$ Steer(x_{rand}, $x_{closest}$);
  if CollisionFree($x_{closest}$, x_{new}) **then**
    $X_{near} \leftarrow$ NearNeighbors($\mathbf{G}$, x_{new});
    $V \leftarrow V \cup \{x_{new}\}$;
    $x_{min} \leftarrow x_{closest}$;
    $c_{min} \leftarrow$ Cost($x_{closest}$) + PixelCost($x_{closest}, x_{new}$);
    foreach $x_{near} \in X_{near}$ **do**
    /* Connect along a minimum-cost path */
      if CollisionFree(x_{near}, x_{new}) **then**
        if Cost(x_{near}) + PixelCost(x_{near}, x_{new}) $< c_{min}$ **then**
          $x_{min} \leftarrow x_{near}$;
          $c_{min} \leftarrow$ Cost(x_{near}) + PixelCost(x_{near}, x_{new});
        end
      end
    end
    $E \leftarrow E \cup \{(x_{min}, x_{new})\}$;
    foreach $x_{near} \in X_{near}$ **do**
    /* Rewire the tree to keep energy minimal */
      if CollisionFree(x_{new}, x_{near}) **then**
        if Cost(x_{new}) + PixelCost(x_{new}, x_{near}) < Cost(x_{near}) **then**
          $x_{parent} \leftarrow$ Parent(x_{near});
          $E \leftarrow (E \setminus \{(x_{parent}, x_{near})\}) \cup \{(x_{new}, x_{near})\}$;
        end
      end
    end
  end
  if $x_{goal(s)}$ ReachedWithAuto-convergence **then**
    return Γ;
  end
end

In order to improve the algorithm efficiency and reduce unnecessary sampling points, we design the pixel-distributed probability for x_{rand}. Let $\mathbb{P}_p$ in Equation (2) as the probability distribution operator, where T_1, T_2 are the relevant hyperparameterized thresholds. $\mathbb{P}_p$ is expressed as:

$$\mathbb{P}_p = \begin{cases} 1 & if \ \ |P_{x_{rand}} - P_0| \le T_1, \\ 0.5 & if \ \ T_1 < |P_{x_{rand}} - P_0| \le T_2, \\ 0 & otherwise, \end{cases} \tag{2}$$

$$P_0 = \alpha * P_{x_{init}} + (1 - \alpha) * P_{x_{goal(s)}}, \quad \alpha \in [0, 1], \tag{3}$$

where P_0 is a constant related to the pixel values of starting point x_{init} and ending point $x_{goal(s)}$, whose pixel values are set to be $P_{x_{init}}$ and $P_{x_{goal(s)}}$ respectively.

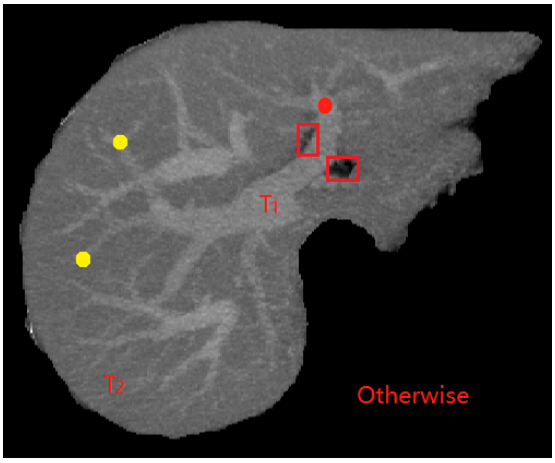

Fig. 1: Thresholds illustration.

According to Equation (2), if $P_{x_{rand}}$(the pixel value of x_{rand}) satisfies $|P_{x_{rand}} - P_0| \le T_1$, as shown in Figure 1, x_{rand} will be inside the liver vessel with a extremely high probability, thus the sampling probability $\mathbb{P}_p$ is set to be 100%. Correspondingly, T_2 is the threshold of the extravascular region. x_{rand} satisfying the second case of Equation (2) owns the distinct pixel difference but can not be confirmed whether its location is intravascular or not with a definite probability, here we set sampling probability $\mathbb{P}_p$ to be 50%. The reason why the sampling probability in this region having distinct pixel differences is not reduced to 0 rashly is to avoid the local minimum problem caused by unreasonable sampling. The black external region of the liver and domains enclosed in the two red rectangles of Figure 1 belong to the apparent obstacles, the sampling probability is 0. The proposed sampling probability operator $\mathbb{P}_p$ can significantly improve the efficiency of Pixel-RRT*, and still, maintain the rationality of results.

2) Cost function: We design the particular cost function: PixelCost in Algorithm 1, which could be regarded as a representation of chasing energy minimum in vascular images, and a new kind of "distance metric" only by calculating the image intensity. In the classical RRT*-related algorithms, the cost function is generally the computation of Euclidean distance of two nodes in the random tree $\mathbf{G}$, which is proverbially used for path planning in games or reality. Nevertheless, the distance-based cost function will not be able to measure the energy

distribution and pixel differences of the image. We propose a novel cost function $\mathbf{C}_p$ in our Pixel-RRT*, defined in Equation (4, 5, 6):

$$\mathbf{C}_p = \mathbf{E}_{external} + \lambda \mathbf{E}_{internal}, \tag{4}$$

$$\mathbf{E}_{external} = \sum_{i=1}^{N} exp(|P_0 - P_i|^n), \tag{5}$$

$$\mathbf{E}_{internal} = \sum_{i=1}^{N-1} exp(|P_i - P_{i+1}|^n), \tag{6}$$

where $n \in \mathbb{Z}^+$, $\lambda \in [0, 1]$, P_0 is the notation of Equation (3), P_i is the pixel value involved by the connecting line between two points of tree $\mathbf{G}$ inputted into `PixelCost`, N is the total number of pixel blocks on the line, and n is usually set to be 1. The first term $\mathbf{E}_{external}$ of $\mathbf{C}_p$ denotes the external energy, which is the accumulation of pixel difference between P_i and P_0. The second term $\mathbf{E}_{internal}$ of $\mathbf{C}_p$ denotes the internal energy of points on the connecting line. Thus, the cost of edges in the tree $\mathbf{G}$ can be measured only depending on image intensity, which avoid the disadvantage of distance-based cost for image analysis. In Figure 2, we give a vivid description about `PixelCost`. We assume A and B are the two arbitrary nodes of the random tree $\mathbf{G}$, which are inputted into the cost function `PixelCost` to compute the cost from A to B. All the pixel blocks involved by the connecting line from A to B are acquired through subdivision interpolation. As is depicted in Figure 2(b), the cyan pixel blocks are P_i of Equation (4), and the total number of them is N. It should be noted that the cyan pixel blocks are obtained with an operation of rounding after interpolation for the sake of decreasing the computational cost, which also does not affect the evaluation and measurement of the cost from A to B.

The computational method of `PixelCost` characterizes the energy variation with different pixel values. If the pixel value approaches to P_0, the cost $\mathbf{C}_p$ is low, on the contrary, it is high. We adopt this cost function `PixelCost` to the basic architecture of RRT*, which can get an optimized trajectory with minimal energy in the process of tree $\mathbf{G}$ expanding and rewiring. Besides, the cost function can ensure the continuity of the final vascular trajectory. We refer to our simulation experiment of Figure 3 to demonstrate the designed cost function. The cost function presents its capacity to help to gain a continuous trajectory with minimal energy(Figure 3(b)). The ongoing trajectory keeps seeking for the nodes whose pixel value is close to the two endpoints to evade the region of high energy(Figure 3(c) and (d)). It can also pass the gray barrier directly to guarantee the minimum cost when having no alternative(Figure 3(d)). In Section III, the more validations of hepatic vessels are illustrated.

3) Multi-goal Strategy: The vasculature system of hepatic vessels gradually produces a hierarchical vascular network along with its growth. Consequentially, a vascular trajectory

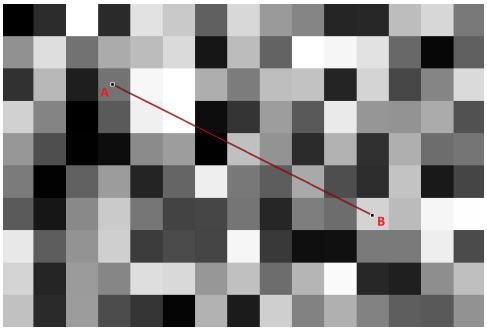

(a) The edge from A to B of random tree $\mathbf{G}$

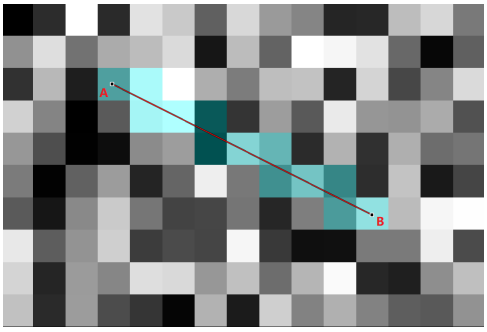

(b) The cyan pixel blocks: P_i lying on edge AB

Fig. 2: (a) and (b): Illustration of the computation of cost function of Pixel-RRT* : `PixelCost`

starting from the trunk will gain multiple bifurcation nodes, endpoints and branches after repetitive bifurcation. In order to better address such practical problems, our Pixel-RRT* adds a multi-goal strategy in the shared random tree $\mathbf{G}$. In the expanding and rewiring of Pixel-RRT* with the constraint of multi-goal, the one closest to the cluster center of all the goals is selected to be the first endpoint, and the remaining unreached goals serve as the next endpoint in sequence. In addition to that, we update the cost of the trajectories having exactly arrived to be 0, so as to ensure the reasonable bifurcation and efficient search of the vascular trajectories.

B. Postprocessing

In this section, we give the postprocessing technique to optimize the trajectory obtained in the above section. Since Pixel-RRT* is based on random sampling to continuously explore and finally obtain the trajectory with minimal energy, such randomness will inevitably lead to jitter of the trajectory. To make the vascular skeleton trajectory smoother and more natural, we propose an adaptively interpolated variational method according to the primary ideas of [37]–[39].

After acquiring the preliminary vascular trajectory with minimal energy via Pixel-RRT*, We redesign a new energy function $E(s)$ of $c(s)$ combined with the variational method as follows:

$$E(s) = \alpha \int_0^1 \|c^{'}(s)\|^2 ds + \beta \int_0^1 \|c^{''}(s)\|^2 ds + \gamma \int_0^1 \|\nabla I(s)\|^2 ds, \tag{7}$$

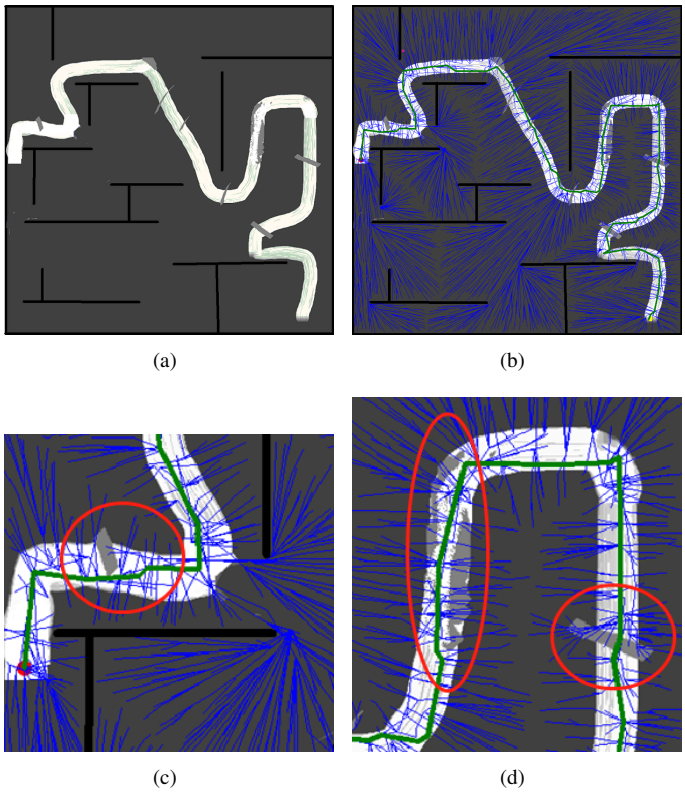

Fig. 3: Effect of cost function `PixelCost`: (a) Input: The simulated image; (b) Output: A final trajectory with minimal cost by evading the region of high cost; (c) Evading the region of high cost; (d) Passing the gray barrier directly to guarantee the minimum cost.

where α , β and γ are real positive weight constants, $c(s)$ is a parameterized curve denoting the preliminary vascular trajectory from Pixel-RRT*, $c^{'}(s)$ and $c^{''}(s)$ are the first derivative and the second derivative with respect to s, denoting the length term and curvature term respectively. $\int_0^1 \|c^{'}(s)\|^2 ds$ evaluates the length of the preliminary vascular trajectory, $\int_0^1 \|c^{''}(s)\|^2 ds$ evaluates the curvature of that, $\int_0^1 \|\nabla I(s)\|^2 ds$ is the potential which relies on image gradient around the vascular trajectory. The postprocessing is to minimize $E(s)$ through adjusting the offset of the parameterized curve, in the process of which a smoother trajectory can be obtained. This postprocessing method can be treated as a kind of active contour model against open curve.

Before variational optimization, an adaptive interpolation by the centripetal Catmull-Rom spline is carried out according to the discrete degree of trajectory-interior nodes. If the consecutive nodes are close, the stage of interpolation will be skipped. The proposed adaptively interpolated variational method can take full advantage of the rule of energy minimization to adjust the location of nodes lying on the trajectory to keep the curve smoother, and simultaneously make sure that the nodes do not move outside the vessel via the constraint of $\int_0^1 \|\nabla I(s)\|^2 ds$ of Equation (7). The following experiments (Section III) validate the feasibility of the proposed postprocessing technique.

III. Experiments and Results

For the sake of convenience when demonstrating our Pixel-RRT* algorithm, we perform the technique of thin slab maximum intensity projection (MIP) [40], [41] on the segmented computed tomography angiography (CTA) image of the liver, where the value of slab is set to be 20 and the projection direction is axial. In consequence, we get the two-dimensional images located in Figure 4(a) and Figure 5(a).

A. Experiment 1: standard validation

The standard validation shows the entire process of proposed methods from Pixel-RRT* to the adaptively interpolated variational method. Figure 4(a) is the input image exhibiting a partial complex hierarchical vascular network of the liver. Figure 4(b) shows the preliminary result derived from Pixel-RRT*, in which the red point and yellow point stand for the starting point and ending point respectively, the blue lines are the edges of random tree $\mathbf{G}$, and the green curve is the result of Pixel-RRT*. The light red curve in Figure 4(c) shows the final result via the adaptively interpolated variational method on basis of Figure 4 (b), which can be seen to become more smoother than the preliminary result. Here, it is remarkable that the distribution of blue lines demonstrates the rationality of the module of Pixel-distributed Random Sampling, which is the foundation of rapid Pixel-RRT*. Overall, this standard experiment proves that our methods achieve sound results. The average elapsed time[1] of this case is about 105 milliseconds after repeating the experiment at least three times.

B. Experiment 2: validation of topological continuity

Topological continuity is a key indicator of evaluating the quality of skeleton trajectory. In this experiment, we validate the continuity of the result from Pixel-RRT*. As is marked in Figure 5(a), there are some obvious fractures and fuzzy pixels in the input image. Figure 5(b) and Figure 5(c) illustrate that Pixel-RRT* can return a continuous trajectory with minimal energy, which can maintain the topological continuity of vasculature. The average elapsed time is about 88 milliseconds after repeating the experiment at least three times.

C. Experiment 3: validation of multi-goal design

In this subsection, we verify the multi-goal design, whose input image is Figure 4(a). Figure 6 covers the corresponding results of two ending points and three ending points. The two cases have shown that our Multi-goal Pixel-RRT* can return multiple trajectories with correct bifurcation. The average elapsed time of these two cases is about 731 milliseconds and 907 milliseconds respectively. In this experiment, the distribution of blue lines demonstrates the rationality of the module of Pixel-distributed Random Sampling more naturally, which also proves that our Pixel-RRT* can build an effective tree structure of hepatic vessels.

[1]All the experiments run on a computer with one Intel i7 CPU@2.8.0 GHz and RAM 16.0 GB.

(a) Input image of Pixel-RRT*

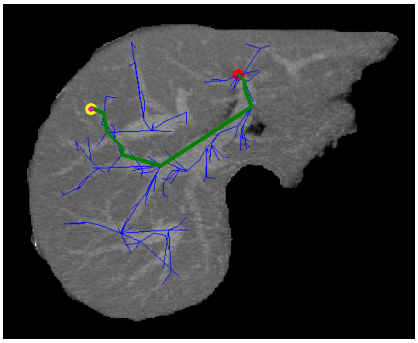

(b) Trajectory via Pixel-RRT*

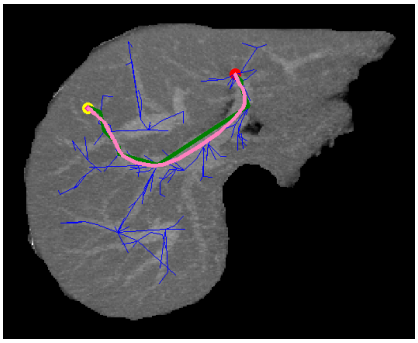

(c) Final optimized trajectory

Fig. 4: Standard validation: (a) input image of Pixel-RRT*, (b) initial trajectory via Pixel-RRT*, (c) final trajectory via adaptively interpolated variational method.

(a) Input image of Pixel-RRT*

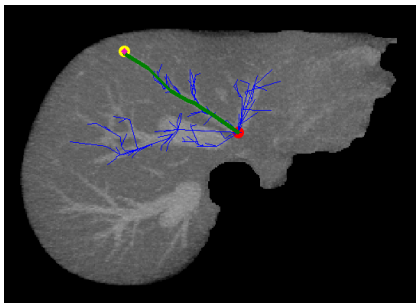

(b) Trajectory via Pixel-RRT*

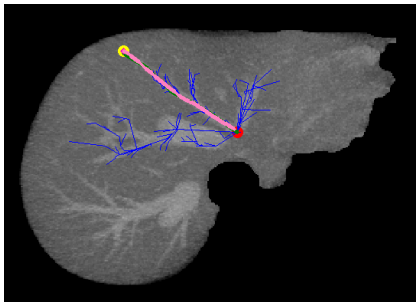

(c) Final optimized trajectory

Fig. 5: Validation of continuity: (a) input image of Pixel-RRT*, (b) initial trajectory via Pixel-RRT*, (c) final trajectory via adaptively interpolated variational method.

The three experiments comprehensively demonstrate the proposed algorithms can successfully search for the reasonable trajectory and then improve the continuous trajectory by postprocessing, which are both corresponding to the principle of energy minimum. These practical examples attest that our novel methods could be used to help us track the skeleton trajectory of hepatic vessels.

D. Evaluation: Algorithm Analysis and Comparison

Without appropriate cost function like `PixelCost` of our Pixel-RRT*, some other classical path planning methods such as A* and PRMs employing Manhatton distance or Euclidean distance can not be successfully applied for the skeleton trajectory search of vascular images. Only based on the prior segmentation results of vessels, these classical distance-based methods can work well, however, which will not be able to avoid the disadvantage of prior segmentation. Moreover, it will be time-consuming to compute the skeleton trajectory after segmentation. Our Pixel-RRT* overcomes these issues, and the acquired skeleton trajectory is directed, whose mechanism of rapidly-exploring tree can also effectively cope with multi-goal search of vascular tree. Another classical approach that can extract skeleton trajectory of blood vessels without prior segmentation is the Fast Marching Minimal Path(FMMP) Method[2]. We make a specific comparison against hepatic vessels in Figure 7. It is remarkable that Pixel-RRT* works well based on the pixel-based cost function, while FMMP doesn't work since its gradient-descent-based cost estimation cannot preferably distinguish the variable image intensity of

[2]Codes: github.com/InsightSoftwareConsortium/ITKMinimalPathExtraction

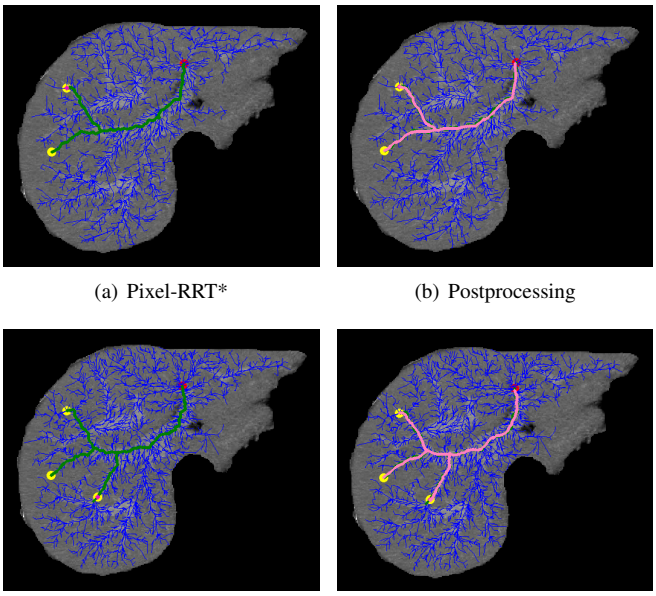

(a) Pixel-RRT* (b) Postprocessing

(c) Pixel-RRT* (d) Postprocessing

Fig. 6: Two cases of Multi-goal Pixel-RRT*.(a) and (b): two goals, (c) and (d): three goals

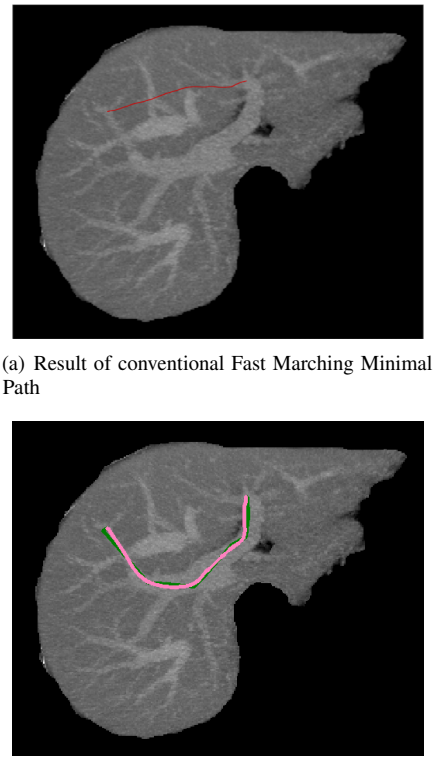

(a) Result of conventional Fast Marching Minimal Path

(b) Result of our Pixel-RRT*

Fig. 7: (a) and (b): Pixel-RRT* VS conventional Fast Marching Minimal Path(FMMP) with same start and end point

hepatic vessels.

In Table I, we make more qualitative comparisons against representative techniques which can acquire the skeleton trajectory of vascular images. The * in the table denotes an additional remark that the corresponding methods can not measure the cost of varying image pixels due to its distance-based cost function. The $+$ shows that the corresponding method can mantain the topological continuity and scale well with problem size respectively, and the $-$ denote the contrary. Pixel-RRT*, other classical RRT*s, and PRMs can scale more effectively with problem size owing to their random sampling for stochastic incremental searches, while Minimal Path and A* discretize the continuous state space with grid searches. Based on the comparisons and analysis, we can find that Pixel-RRT* own the best performance. Besides, the algorithmic mechanism of expanding tree in our Pixel-RRT* can support multi-goal more readily.

TABLE I: Comparisons for other representative methods and Pixel-RRT*

Methods	Complexity	Continuity	Scalability	Remark
Pixel-RRT*	$O(n)$	$+$	$+$	
Other RRT*s	$O(n)$	$+$	$+$	$*$
FMMP	$O(nlogn)$	$+$	$-$	
A*	$O(nlogn)$	$+$	$-$	$*$
PRMs	$O(nlogn)$	$+$	$+$	$*$

IV. Discussion and Conlusion

The proposed methods in our paper mainly cover the Pixel-RRT* with a novel cost function and the adaptively interpolated variational method. The theoretical analysis and the practical examples demonstrate that our methods can serve crucial functions in the fields such as exploring the skeleton trajectory of blood vessels. The posterior parts of small vasculature are blurry and occasionally disconnected in most cases. Pixel-RRT* exerts the own design of minimum-cost and topological continuity to successfully tackle these difficulties, and our methods can implement multi-trajectory analysis with right bifurcation nodes, particularly when coping with the luxuriant vascular images that can not be clearly observed by the naked eye. Furthermore, our methods will be able to be extended to the trajectory tracking and navigation of other vasculatures besides hepatic vessels, such as trachea, intestinal tract and plant veins.

Pixel-RRT* can also be applied for path planning in other kinds of digital images thanks to its pixel-based cost function. Pixel-RRT* will return a corresponding energy-minimal continuous path according to the two imported endpoints. To some extent, Pixel-RRT* can also guide the segmentation of vascular tissues because of the property of maintaining topological continuity. In most cases, our methods can achieve the desired result without any image preprocessing. If necessary, please select some shape-preserving local contrast enhancement methods.

In the future, we would optimize the current variational model through adding an automatic radius term to adjust the final trajectory to be the tubular centerline thoroughly, then our

Pixel-RRT* can segment the vessels and acquire the skeleton simultaneously meeting the principle of global minimization and topological continuity.

V. Acknowledgements

Our work presented in this paper is partially supported by the National Natural Science Foundation of China under Grant No.91630311 and the Natural Science Foundation of Zhejiang Province under Grant No.LSD19H180005.

References

[1] T. Bär, *The vascular system of the cerebral cortex*. Springer Science & Business Media, 2012, vol. 59.

[2] L. Coultas, K. Chawengsaksophak, and J. Rossant, "Endothelial cells and vegf in vascular development," *Nature*, vol. 438, no. 7070, pp. 937–945, 2005.

[3] C. Debbaut, P. Segers, P. Cornillie, C. Casteleyn, M. Dierick, W. Laleman, and D. Monbaliu, "Analyzing the human liver vascular architecture by combining vascular corrosion casting and micro-ct scanning: a feasibility study," *Journal of anatomy*, vol. 224, no. 4, pp. 509–517, 2014.

[4] H. Blum *et al.*, *A transformation for extracting new descriptors of shape*. MIT press Cambridge, 1967, vol. 4.

[5] M. Li, S. Chen, X. Chen, Y. Zhang, Y. Wang, and Q. Tian, "Actional-structural graph convolutional networks for skeleton-based action recognition," in *Proceedings of the IEEE Conference on Computer Vision and Pattern Recognition*, 2019, pp. 3595–3603.

[6] R. B. Martin, "Functional adaptation and fragility of the skeleton," in *Bone Loss and Osteoporosis*. Springer, 2003, pp. 121–138.

[7] Z. Zhou and A. Venetsanopoulos, "Morphological skeleton representation and shape recognition," in *ICASSP-88., International Conference on Acoustics, Speech, and Signal Processing*. IEEE Computer Society, 1988, pp. 948–949.

[8] E.-J. Ong and S. Gong, "Tracking hybrid 2d-3d human models from multiple views," in *Proceedings IEEE International Workshop on Modelling People. MPeople'99*. IEEE, 1999, pp. 11–18.

[9] L. D. Cohen and R. Kimmel, "Global minimum for active contour models: A minimal path approach," *International journal of computer vision*, vol. 24, no. 1, pp. 57–78, 1997.

[10] O. Wink, W. J. Niessen, and M. A. Viergever, "Multiscale vessel tracking," *IEEE Transactions on Medical Imaging*, vol. 23, no. 1, pp. 130–133, 2004.

[11] T. Deschamps and L. D. Cohen, "Fast extraction of minimal paths in 3d images and applications to virtual endoscopy," *Medical image analysis*, vol. 5, no. 4, pp. 281–299, 2001.

[12] K. Palágyi, "A 3d fully parallel surface-thinning algorithm," *Theoretical Computer Science*, vol. 406, no. 1-2, pp. 119–135, 2008.

[13] L. Serino, C. Arcelli, and G. S. di Baja, "On the computation of the (3, 4, 5) curve skeleton of 3d objects," *Pattern Recognition Letters*, vol. 32, no. 9, pp. 1406–1414, 2011.

[14] M. Wan, Z. Liang, Q. Ke, L. Hong, I. Bitter, and A. Kaufman, "Automatic centerline extraction for virtual colonoscopy," *IEEE transactions on medical imaging*, vol. 21, no. 12, pp. 1450–1460, 2002.

[15] E. Bas and D. Erdogmus, "Principal curves as skeletons of tubular objects," *Neuroinformatics*, vol. 9, no. 2-3, pp. 181–191, 2011.

[16] T. Xu, D. Vavylonis, and X. Huang, "3d actin network centerline extraction with multiple active contours," *Medical image analysis*, vol. 18, no. 2, pp. 272–284, 2014.

[17] T. F. Sherman, "On connecting large vessels to small. the meaning of murray's law." *The Journal of general physiology*, vol. 78, no. 4, pp. 431–453, 1981.

[18] D. L. Cohn, "Optimal systems: I. the vascular system," *The Bulletin of mathematical biophysics*, vol. 16, no. 1, pp. 59–74, 1954.

[19] P. Bruyninckx, D. Loeckx, D. Vandermeulen, and P. Suetens, "Segmentation of lung vessel trees by global optimization," in *Medical Imaging 2009: Image Processing*, vol. 7259. International Society for Optics and Photonics, 2009, p. 725912.

[20] ——, "Segmentation of liver portal veins by global optimization," in *Medical Imaging 2010: Computer-Aided Diagnosis*, vol. 7624. International Society for Optics and Photonics, 2010, p. 76241Z.

[21] H. Ronellenfitsch and E. Katifori, "Global optimization, local adaptation, and the role of growth in distribution networks," *Physical review letters*, vol. 117, no. 13, p. 138301, 2016.

[22] S. M. LaValle and J. J. Kuffner Jr, "Randomized kinodynamic planning," *The international journal of robotics research*, vol. 20, no. 5, pp. 378–400, 2001.

[23] S. M. LaValle, "Rapidly-exploring random trees: A new tool for path planning," 1998.

[24] M. Du, T. Mei, H. Liang, J. Chen, R. Huang, and P. Zhao, "Drivers' visual behavior-guided rrt motion planner for autonomous on-road driving," *Sensors*, vol. 16, no. 1, p. 102, 2016.

[25] A. Bhatia and E. Frazzoli, "Incremental search methods for reachability analysis of continuous and hybrid systems," in *International Workshop on Hybrid Systems: Computation and Control*. Springer, 2004, pp. 142–156.

[26] J. Cortés, L. Jaillet, and T. Siméon, "Molecular disassembly with rrt-like algorithms," in *Proceedings 2007 IEEE International Conference on Robotics and Automation*. IEEE, 2007, pp. 3301–3306.

[27] M. Zucker, J. Kuffner, and M. Branicky, "Multiple rrts for rapid replanning in dynamic environments," in *IEEE Conference on Robotics and Automation*, 2007.

[28] S. Karaman and E. Frazzoli, "Sampling-based algorithms for optimal motion planning," *The international journal of robotics research*, vol. 30, no. 7, pp. 846–894, 2011.

[29] J. D. Gammell, S. S. Srinivasa, and T. D. Barfoot, "Informed rrt*: Optimal sampling-based path planning focused via direct sampling of an admissible ellipsoidal heuristic," in *2014 IEEE/RSJ International Conference on Intelligent Robots and Systems*. IEEE, 2014, pp. 2997–3004.

[30] A. H. Qureshi and Y. Ayaz, "Intelligent bidirectional rapidly-exploring random trees for optimal motion planning in complex cluttered environments," *Robotics and Autonomous Systems*, vol. 68, pp. 1–11, 2015.

[31] A. H. Qureshi, K. F. Iqbal, S. M. Qamar, F. Islam, Y. Ayaz, and N. Muhammad, "Potential guided directional-rrt* for accelerated motion planning in cluttered environments," in *2013 IEEE International Conference on Mechatronics and Automation*. IEEE, 2013, pp. 519–524.

[32] A. H. Qureshi, S. Mumtaz, K. F. Iqbal, B. Ali, Y. Ayaz, F. Ahmed, M. S. Muhammad, O. Hasan, W. Y. Kim, and M. Ra, "Adaptive potential guided directional-rrt," in *2013 IEEE International Conference on Robotics and Biomimetics (ROBIO)*. IEEE, 2013, pp. 1887–1892.

[33] K. Naderi, J. Rajamäki, and P. Hämäläinen, "Rt-rrt* a real-time path planning algorithm based on rrt," in *Proceedings of the 8th ACM SIGGRAPH Conference on Motion in Games*, 2015, pp. 113–118.

[34] P. E. Hart, N. J. Nilsson, and B. Raphael, "A formal basis for the heuristic determination of minimum cost paths," *IEEE transactions on Systems Science and Cybernetics*, vol. 4, no. 2, pp. 100–107, 1968.

[35] L. E. Kavraki, P. Svestka, J.-C. Latombe, and M. H. Overmars, "Probabilistic roadmaps for path planning in high-dimensional configuration spaces," *IEEE transactions on Robotics and Automation*, vol. 12, no. 4, pp. 566–580, 1996.

[36] L. Schmid, M. Pantic, R. Khanna, L. Ott, R. Siegwart, and J. Nieto, "An efficient sampling-based method for online informative path planning in unknown environments," *IEEE Robotics and Automation Letters*, vol. 5, no. 2, pp. 1500–1507, 2020.

[37] M. Kass, A. Witkin, and D. Terzopoulos, "Snakes: Active contour models," *International journal of computer vision*, vol. 1, no. 4, pp. 321–331, 1988.

[38] E. Catmull and R. Rom, "A class of local interpolating splines," in *Computer aided geometric design*. Elsevier, 1974, pp. 317–326.

[39] C. Yuksel, S. Schaefer, and J. Keyser, "Parameterization and applications of catmull–rom curves," *Computer-Aided Design*, vol. 43, no. 7, pp. 747–755, 2011.

[40] M. Prokop, M. Galanski, and A. J. Van Der Molen, *Spiral and multislice computed tomography of the body*. Thieme, 2003.

[41] M. Remy-Jardin, J. Remy, D. Artaud, F. Deschildre, and A. Duhamel, "Diffuse infiltrative lung disease: clinical value of sliding-thin-slab maximum intensity projection ct scans in the detection of mild micronodular patterns." *Radiology*, vol. 200, no. 2, pp. 333–339, 1996.